Gold supported on CuO_x/CeO_2 catalyst for the purification of hydrogen by the CO preferential oxidation reaction (PROX)

O.H. Laguna*[1], W.Y. Hernández[1], G. Arzamendi[2], L.M. Gandía[2], M.A. Centeno[1], J.A. Odriozola[1]

[1] Instituto de Ciencia de Materiales de Sevilla, Centro Mixto Universidad de Sevilla-CSIC, Avenida Américo Vespucio 49, 41092, Seville, Spain

[2] Departamento de Química Aplicada, Edificio de los Acebos, Universidad Pública de Navarra, Campus de Arrosadía s/n, E-31006, Pamplona, Spain

* Corresponding author: oscarhernando.laguna@ehu.es

Tel: +34 954489221

Abstract

Hydrogen produced from the conversion of hydrocarbons or alcohols contains variable amounts of CO that should be removed for some applications such as feeding low-temperature polymer electrolyte membrane fuel cells (PEMFCs). The CO preferential oxidation reaction (PROX) is particularly well-suited for hydrogen purification for portable and on-board applications. In this work, the synthesis and characterization by XRF, BET, XRD, Raman spectroscopy and H_2-TPR of a gold catalyst supported on a copper-cerium mixed oxide (AuCeCu) for the PROX reaction are presented. The comparison of this catalyst with the copper-cerium mixed oxide (CeCu) revealed that the experimental procedure used for the deposition of gold gave rise to the loss of reducible material by copper lixiviation. However, the AuCeCu solid was more active for CO oxidation at low temperature. A kinetic study has been carried over the AuCeCu catalyst for the PROX reaction and compared with that of the CeCu catalyst. The main difference between the models affected the contribution of the CO adsorption term. This fact may be related to the surface electronic activity produced by the interaction of the cationic species in the AuCeCu solid, able to create more active sites for the CO adsorption and activation in the presence of gold.

Keywords: gold catalyst; copper-cerium oxide; hydrogen; PROX, CO oxidation; kinetics

1. Introduction

Nowadays, important efforts are being focused on developing renewable energy sources that can reduce our dependence on fossil fuels [1]. Although hydrogen is not a primary energy source, it seems a suitable fuel in the long-term since its clean combustion prevents the emission of carbon-based pollutants and/or greenhouse gases [2]. Hydrogen production by the reforming of hydrocarbons either from fossil or renewable origin seems to be the best option in the short-term; however, the produced reformate is not pure H_2 but a mixture of different compounds, being H_2, H_2O and carbon oxides (CO and CO_2) the main ones [3]. If the reformate is intended to fuel low-temperature PEMFCs, the CO content must be below 10-20 ppm in order to prevent the poisoning of the Pt-based PEMFC electrodes [4]. This is achieved by the combination of different clean-up processes, typically by the high and low-temperature Water-Gas Shift reactions (HT-WGS and LT-WGS, respectively) that allow decreasing the CO levels to 0.5-1 vol. % [5-7]) and a final step to reduce the CO concentration to an acceptable level. The CO preferential oxidation with air (PROX) of the pre-cleaned reformate is a cheap and effective final step since it can be performed at atmospheric pressure and the range of working temperatures matches the one at which PEMFCs [8]. Additionally it is among the preferred technologies for small-scale fuel processors for portable and on-board applications and auxiliary power units [9].

Along with the CO oxidation (Eq. 1), the H_2 oxidation (Eq. 2), the WGS (Eq. 3) and the CO and CO_2 hydrogenation (methanation) reactions (Eqs. 4 and 5) can affect the final composition of the system.

$CO+\frac{1}{2}O_2 \rightarrow CO_2$	ΔH° = -283 kJ/mol	(Eq. 1)
$H_2+\frac{1}{2}O_2 \rightarrow H_2O$	ΔH° = -242 kJ/mol	(Eq. 2)
$CO + H_2O \leftrightarrows CO_2 + H_2$	ΔH° = -41.4 kJ/mol	(Eq. 3)
$CO + 3H_2 \leftrightarrows CH_4 + H_2O$	ΔH° = -207 kJ/mol	(Eq. 4)
$CO_2 + 4H_2 \leftrightarrows CH_4 + 2H_2O$	ΔH° = -165.5 kJ/mol	(Eq. 5)

Among these processes, the H_2 oxidation and the WGS and its reverse reaction (R-WGS) are the most influential ones over the selectivity due to the low temperatures at which the PROX reaction is usually carried out (< 300 °C) [10]. It is clear that the performance of a specific PROX catalyst should include high conversions and selectivities towards CO oxidation.

Several catalytic systems have been reported for use in the PROX reaction; they can be classified into three groups [11]: i) Pt, Ru and Rh supported catalysts [12,13]; ii) gold supported catalysts [14,15] iii) and copper-cerium oxide based catalysts. The last group has been thoroughly studied [8,16,17] and is well-known for presenting considerably higher selectivity to CO oxidation than the Pt-based catalysts at comparable conversion levels. As regards the gold supported catalysts, they are very active, especially at low temperature which is one of the challenges to be overcome when designing PROX catalysts [14,15]. Combining copper and gold on several catalytic supports has been considered in some recent studies [18-23]. In these works, a synergistic effect between gold and copper was found and related to electronic interactions between both metals. Since gold and copper have the same crystal structure and similar lattice spacing, they are miscible in all proportions and may form stable intermetallic alloys with 3:1, 1:1 and 1:3 molar Au:Cu ratios. The enhancement of the catalytic activity by the interaction of copper and gold strongly depends on the particle size which, at the same time, depends on the amount of Cu and Au, the Au:Cu ratio and the synthesis procedure. In general, it is considered that alloying gold with copper produces more stable metallic particles since copper is segregated on the surface forming copper oxides and hindering gold sintering under oxidizing conditions. However, in most of these cases, large Au:Cu ratios (above 0.33) are used. Particularly on ceria support, Fonseca et al. [24] have demonstrated that an Au-CuO_x/CeO_2 solid with similar gold and CuO_x contents (around 1 wt. %) presented a performance in the PROX reaction intermediate between the 1.1 wt. % CuO_x/CeO_2 and the 1 wt. % Au/CeO_2 catalysts, keeping good CO conversion and selectivity levels. The principal contributions of gold observed by these authors were a lower inhibiting effect of CO_2 and avoiding the deactivation by H_2O. However, to our knowledge, the effect of small additions of gold to very active high-loaded CuO_x/CeO_2 PROX catalysts has not been reported.

As concerns the kinetics, several models have been proposed for the PROX reaction over CuO_x-CeO_2 [25-32]. The formulation of adequate kinetic models is a key step on designing and scaling up of PROX units [33], thus being fundamental for the practical applications of this H_2 cleaning technology. The success of a kinetic model in describing the experimental data depends, among other aspects, on taking into account all the relevant processes that may occur during the PROX reaction. Choi et al. [27] pointed out the importance of considering the contribution of the CO and H_2 oxidations and the WGS reaction. Both Langmuir-Hinshelwood (LH) [34,35] and Mars-Van Krevelen type [31] kinetic equations have been found valid for describing the PROX reaction over CuO_x/CeO_2.

Within this general scenario, we present in this work the synthesis, characterization and testing of a high-loaded (10 wt. %) CuO_x/CeO_2 solid and a gold catalyst (1 wt. %) prepared from it, in the oxidation of CO (TOX) and preferential oxidation of CO in the presence of H_2 (PROX) reactions. It is intended this way comparing the CO oxidation performance of the catalysts under different O_2 availability conditions which can be interesting to better understand the PROX reaction in the presence of these solids and design more efficient catalysts. Additionally, a kinetic model is formulated for the Au-CuO_x/CeO_2 catalyst in the PROX reaction and compared to that for the CuO_x/CeO_2 solid that was reported in a previous study [36].

2. Materials and Methods

2.1. Synthesis of the catalysts

The CuO_x/CeO_2 (with 10 CuO wt.% and 90 CeO_2 wt.%) catalyst was prepared by coprecipitation method [36,37]. The required amounts of $Cu(NO_3)_2{\cdot}3H_2O$ (Fluka®) and $Ce(NO_3)_3{\cdot}6H_2O$ (Alfa Aesar®) were dissolved in distilled water forming a 0.5 M solution. After mixing under vigorous stirring, a NaOH solution (2 M) was added dropwise until a stable pH of 9. The obtained precipitate was filtered and washed with distilled water in order to eliminate sodium and nitrate ions. Then, it was dried overnight at 60 °C and finally calcined at 300 °C (10 °C/min) for 2 h. The resulting solid was named CeCu and a portion of it was used as support for preparing the gold catalysts through the deposition–precipitation method [14]. The adequate amount of $HAuCl_4{\cdot}3H_2O$ (Alfa Aesar) to obtain a loading of 1 wt. % Au, was dissolved in deionized water (6.0×10^{-4} M) and the pH of the solution adjusted to 8 by addition of NaOH 0.1 M with an automatic system of measurement and titration (CRISON® pH-Burette 24). This pH value has been reported as adequate for a successful deposition of gold on ceria surfaces [38,39]. The solution was heated to 70 °C and then the support was added and kept under continuous stirring for 20 min. The solid obtained after filtration was washed with distilled water several times (until the disappearance of chloride and sodium ions), then dried overnight at 100 °C and calcined for 2 h at 300 °C. The final catalyst was named AuCeCu.

2.2. Characterization techniques

The elemental composition of the samples was determined by X-ray fluorescence (XRF) spectrometry in a Panalytical® AXIOS PW4400 sequential spectrophotometer with Rh tube as source of radiation. The measurements were performed onto pressed pellets containing 6 wt. % wax.

The textural properties were studied by N_2 adsorption/desorption measurements at liquid N_2 temperature in a Micromeritics® ASAP 2010 apparatus. Before analysis, the samples were degassed at 150 °C for 2 h under vacuum.

Powder X-ray diffraction (XRD) patterns were recorded on a Siemens® D500 diffractometer, using Cu K_α radiation (40 mA, 40 kV), with 0.017° step size and 275 s of step time, over a 2θ range from 10 to 90°. For the crystallite size calculation, the Scherrer equation was applied over the most intense XRD peak around 28.5 °2θ, corresponding to the (111) CeO_2 planes, by using the software X'pert HighScore 1.0f. For correcting the instrumental effects, a pattern of Si was used, with a particle size above 2000 Å, and a line broadening at half maximum intensity (FWHM) = 0.1, associated to the XRD line at 28.37 °2θ for the (111) crystallographic plane.

Raman spectra were recorded in a dispersive Horiva Jobin Yvon LabRam HR800 Confocal Raman Microscope with a green laser (532.14 nm) working at 5 mV power and using a 600 grooves/mm grating. The microscope used a 50x objective with a confocal pinhole of 1000 µm.

Temperature Programmed Reduction (TPR) experiments were carried out in a conventional quartz reactor connected to a thermal conductivity detector (TCD). The reactive gas stream (5 vol. % H_2 in Ar) was flowed at 50 ml/min over 50 mg of sample and the temperature raised at 10 °C/min from room temperature to 900 °C. A molecular sieve 13X was used to retain the reduction products, mostly H_2O and CO_2. Quantitative analysis was done by integration of the reduction signal and comparison with hydrogen consumption of a CuO reference.

2.3. Catalytic activity measurements and kinetic analysis

Chemical reactivity for the total CO oxidation (TOX) has been used as a characterization tool for surface oxygen mobility. For this purpose the solids (80 mg with 100 µm <ø<200 µm particle size) were pre-treated for 1 h at 300 °C in a 30 ml/min activation flow of 21 vol.% O_2 balanced in He. The light-off curves (from room temperature to 400 °C, 5 °C/min) were obtained passing a 42 mL/min feed-stream containing 3.4 vol. % CO and 21 vol. % O_2 balanced in He. The reaction was carried out in a conventional continuous flow U-shaped quartz reactor working at atmospheric pressure placing the catalyst between glass wools. The reaction products were analysed by mass spectrometry in a Balzers® Thermostar equipped with software Balzers® QuadstarTM 22 [40]. This software allows quantification of CO, O_2 and CO_2 by continuously monitoring the selected m/z signals (28, 32 and 44, respectively, previously

calibrated) as a function of time and related the observed intensity to that of helium (m/z=4) used as an internal standard.

Prior to the kinetic study of the analyzed catalysts in the PROX reaction, catalytic tests were carried in order to confirm the oxidizing ability of the prepared materials after the inclusion of H_2 in the feed-stream. For that purpose a tubular stainless steel reactor (9 mm inner diameter) at atmospheric pressure was employed, using 100 ml/min of a feed-stream containing 2 vol. % CO, 1 vol. % O_2, 50 vol. % H_2 and N_2 as balance [14]. In order to minimize hot spots, fresh catalyst powders (100 mg) were diluted with crushed inert glass (650 mg) with the same particle size until obtaining of a bed length of 5 - 8 mm. Before reaction, samples were activated for 1 h at 300 °C with a 21 vol. % O_2 in N_2 flow (30 mL/min). Products and reactants were separated and quantified by on-line gas chromatography (Varian® CP-4900), equipped with Porapak® Q and Molecular Sieve 5A columns and a TCD detector.

Concerning the kinetic study for the PROX reaction of the prepared solids, a series of experiments were performed in the micro packed-bed reactor described above, that was assumed to be isothermal and plug-flow, which is typically assumed in these cases, considering an adequate flat velocity profile and negligible axial dispersion effects according to the criteria described by Rase [41]. The measured CO and O_2 conversions and selectivity data were fitted to the kinetic models using the Nelder and Mead [42,43] algorithm of direct search furnished by the DBCPOL optimization subroutine in the IMSL library. The catalytic experiments were carried using three series of different feed-stream compositions (see Table 1). In the first group of experiments (compositions 1-3) only the O_2 concentration was modified. For the second series (compositions 4-6) only the CO content was changed. Finally, with compositions 7-10, the presence of CO_2 and H_2O was considered.

The CO conversion and the selectivity for CO oxidation were calculated according to equations 6 and 7, respectively, where F_{COin} and F_{O2in} are the molar flow rates of CO and O_2 in the feed stream and F_{COout} and F_{O2out} are those at the reactor outlet.

$$\text{CO conversion (\%)} = \frac{F_{CO_{in}} - F_{CO\,out}}{F_{CO_{in}}} \times 100 \qquad \text{(Eq. 6)}$$

$$\text{Selectivity to CO oxidation (\%)} = \frac{F_{CO_{in}} - F_{CO_{out}}}{2(F_{O_{2in}} - F_{O_{2out}})} \times 100 \qquad \text{(Eq. 7)}$$

3. Results and discussion

3.1. Physico-chemical characterization

The chemical composition of the prepared solids and their textural properties are presented in Table 2. Copper content is expressed both as CuO wt. % and Cu at. % in order to facilitate the comparison with results reported in literature.

The CeCu solid exhibits an excess of 5 wt. % CuO with respect to the intended value (10 CuO wt. %). This difference may be due to a selective precipitation of some cationic species during the synthesis procedure because of the differences in the solubility products of $Ce(OH)_3$ (pK = 21.19 – 24.40) and $Cu(OH)_2$ (pK = 12.8) [44]. The deposition of gold induces a loss of copper. Probably, when the CeCu solid was dispersed in the solution of gold, some copper species were re-dissolved and, later, lost during the washing step.

However, the final gold loading is very similar to the target value confirming the successful application of the deposition-precipitation method for preparing gold-supported catalysts over CeO_2-based systems [14]. The final Au/Cu molar ratio is 0.03.

As concerns the textural properties, there are no big differences between both solids, although a slight increment in the pore volume and the average pore size is observed in the case of the gold catalyst. This fact has been previously reported in other Au-supported systems and has been attributed to the introduction of gold particles into the porous structure of the support [14,45].

The XRD patterns of the studied materials are presented in Figure 1. For the sake of comparison, the pattern of pure CeO_2 obtained through a procedure similar to that described in section 2.1 has been included. The observed reflections correspond to the *c*-CeO_2 fluorite structure (JCPDS 00-034-0394). No signals may be attributed to any crystalline phase containing Cu or Au and the presence of these metals does not modify the position of the main reflections, suggesting no solid solution formation. Particularly, the absence of signals due to copper containing species may be attributed to their amorphous character or to their high dispersion at the CeO_2 surface. However the segregation of the copper containing phases seems clear.

Zhu et al. [46] also studied CuO-CeO_2 mixed systems prepared by hydrothermal method with different copper contents (recalculated from the data of that paper as 8, 13, 17 and 23 Cu at. %). The authors observed by XRD the segregation of CuO only for the highest copper contents (17 and 23 Cu at. %), which are very close to the Cu content of the AuCeCu solid in this work (see Table 2). Although Zhu et al. [46] associated the absence of CuO XRD reflections to the high dispersion of such species in the cases of low copper content, the existence of trace copper and cerium solid solution formation was not discarded at all because of the broadening of the CeO_2 reflections. Similarly, Mariño et al. [47,48] studied a series of CuO_x/CeO_2 catalysts prepared by the urea thermal decomposition method with copper contents up to 60 at.% and they also indicated that the solid solution could be present even if it were hardly detectable by XRD. Moreover, a good CuO-CeO_2 interdispersion has been achieved with the preparation method, avoiding the generation of big CuO crystallites for Cu contents up to 40 at. %. These observations point out the strong influence of the synthesis procedure over the crystallite domain size of the segregated copper species, as was highlighted by Mariño et al. [48]. In our case, taking into account the copper loading, the absence of any copper oxide reflections, the hardly detectable modification of the CeO_2 diffraction lines, and results reported for other CuO_x/CeO_2 systems, we propose the existence of highly dispersed copper oxide species over the CeO_2 surface. Consequently the presence of amorphous copper species is discarded. The solid solution in the CeCu and AuCeCu solids is hardly observable at least through the experimental techniques employed in the present work.

Concerning the absence of reflections due to the presence of gold, it may be due to its high dispersion and/or to the low gold content (0.9 wt. %). This observation agrees with that reported for a similar gold-loaded (1 wt. %) Au-Ce-Cu system but with a higher Au/Ce ratio [24]. Although no reflections are detected in the XRD profiles of the catalysts due to the presence of copper or gold, the probably interaction between both catalysts may result in the formation of Au-Cu solid solution. Nevertheless additional experimental techniques are required in order to confirm this assumption.

On the other hand, the crystalline domain size calculated with the Scherrer equation (Figure 1) points out a slight decrease due to the interaction between Cu and Ce species. This result is in good agreement with those presented in a previous study on Zr, Zn and Fe-doped ceria [14], where it was concluded that the presence of heteroatoms, even those forming segregated phases, retards the nucleation of the CeO_2 during the calcination stage. The introduction of

gold scarcely modifies the crystallite size, probably because it was deposited after the stabilization of CeCu by calcination at 300 °C.

As for the Raman spectra of the studied solids, these are presented in Figure 2 including the spectra of pure CeO_2, for the sake of comparison. The CeCu presents the typical signals of CeO_2 [14,37,49,50]. The most intense one, centered at 463 cm^{-1}, corresponds to the F_{2g} band and the signal at 612 cm^{-1} is due to the presence of oxygen vacancies (Ov). Comparing the mixed oxide (CeCu) with the bare CeO_2, there is a considerable increase of the oxygen vacancies signal in the system with copper. The oxygen vacancies are punctual defects of the cubic structure of CeO_2 that promote the tetragonalization of a portion of the ceria by the presence of Ce^{3+} cations especially at the surface. The tetragonalization of the cubic structure by the presence of Ce^{3+} species may be confirmed by the broad and small signal centered at 279 cm^{-1} [51]. The promotion of the oxygen vacancies population by the inclusion of copper species is in good agreement with that widely established by different authors whose demonstrated that the doping of the cerium oxide results in the promotion of oxygen vacancies [14,37,40,52]. Such promotion of oxygen vacancies may be produced throughout the solid solution formation as in the case of Ce-Zr or Ce-Fe systems or by the surface interaction between segregated oxides as in the case of CeO_2-ZnO as we recently presented in literature [14].

Concerning the gold catalyst, the most relevant feature of the Raman spectrum is the absence of the Ov signal, confirming the interaction between gold particles and the oxygen vacancies in CeO_2 [14,53]. It has been widely accepted that oxygen vacancies act as preferential sites for the deposition of gold nanoparticles, increasing their dispersion over the CeO_2. In the solids of the present study, the contact between the copper and cerium species at the surface allows increasing the concentration of oxygen vacancies (see Figure 2), and a probable Au-Ce-Cu interaction in the surface of the AuCeCu catalyst should not be dismissed entirely.

Another interesting observation is that the presence of gold promoted a slight red shift and a narrowing of the F_{2g} Raman signal respect to that of CeCu. Many authors have probed the incidence of several factors such as the particle size [54], the modification of the cell parameters or the alteration of the electronic environment of the cubic structure [55] on the shape and position of the F_{2g} signal in ceria-based materials. Although the lower crystallite size of the gold sample (Figure 1) could explain the observed differences [35], the principal changes in the Raman signals must be correlated with the promotion of oxygen vacancies over the

CeO_2 surface by its interaction with the copper species and then, the vanishing of these oxygen vacancies by the deposition of gold. When oxygen vacancies are produced in the CeO_2 an important modification of the nature of f electrons namely from valence to core-like, occurs, as was discussed by Ganduglia-Pirovano et al. [56]. Therefore, after the deposition of gold nanoparticles over the CeCu surface, should not be ruled out a new alteration of the electronic properties of the support by an interaction between the three elements gold, copper and cerium.

The TPR profiles of the studied solids are presented in Figure 3. In the case of the CeCu sample, there are two small and broad signals with maxima at 774 °C and 897 °C which can be associated to the reduction of bulk Ce^{4+} species, and an intense signal at 201 °C due principally to the reduction of the copper species [48,57-59]. However, for this low temperature reduction process (LTP $\sim$ 201 °C) the experimental H_2 consumption calculated with the area of the peak, is higher than the theoretical H_2 consumption for the complete reduction of the copper species, assuming that all of them are as Cu^{2+} (see Table 3). From this result it can be inferred that the simultaneous reduction of copper and some Ce^{4+} cations is produced at low temperature in the CeCu solid. In previous studies about the reducibility of the CeO_2 it has been widely established that the reduction of Ce^{4+} at low temperature is occurring at the surface of the oxide from 400 to 500 °C [14,40], which agrees with the fact that the Ce^{3+} reduced species are preferentially placed at the surface of the material in order to reduce the free Gibbs energy, as was discussed by Gellings et al. [60]. However, the CeCu has exhibited the reduction of Ce^{4+} species at temperatures below 300 °C, which would be confirming that the interaction between the copper species and the surface of the CeO_2 results in an easier reduction and stabilization of Ce^{3+} species at low temperatures. Consequently, the increasing of the oxygen vacancies population observed in the Raman spectroscopy (Figure 2) can be directly related with the improvement of the reducibility of this material.

Concerning the narrowness of the LTP of the CeCu, it could be associated to the particle size of the species containing copper. Sirichaiprasert et al. [61], have studied the reduction of CuO deposits over the CeO_2, establishing that such CuO deposits may exhibit more than a maximum when their particle size is high. In that case, the reduction of surface and bulk Cu^{2+} species is clearly differentiated by two low temperature signals [61]. If our CeCu solid presents some CuO deposits, the narrowness of the LTP would be due to their low particle size. This result would be in agreement with a high dispersion of the species with copper and may be confirming the absence of XRD reflexions by copper oxides.

On the other hand, the possible H_2 spillover effects over the reducibility of the CeCu system must not be discarded. Araújo et al. [62] have prepared catalysts for the PROX reaction and they proposed that H_2 might be dissociatively adsorbed on CuO and the hydrogen atoms can spillover to the CeO_2 support, enhancing the reducibility of Ce^{4+} species. This is in good agreement with our results and would explain the observed excess of H_2 consumption in the LTP compared to the theoretical one for the reduction of all the CuO species (Table 3), and suggesting the simultaneous reduction of some other species

The AuCeCu solid presents a similar TPR profile, with a high temperature peak at 794 °C, associated to the reduction of bulk Ce^{4+} species, and a low temperature one at 241 °C. The observed shift of 40 °C to higher reduction temperatures and the lower area (lower H_2 consumption) of the LTP compared to that of CeCu (Figure 3) may be related with the detected loss of copper species after gold deposition. The lower amount of copper in AuCeCu results in a decrease of the reducible material content, which can explain the lower area of the peak, while the loss of cerium and copper interactions reduces the synergy between both metals. Consequently, although copper is still in a large excess respect to gold species, the decreasing of the copper loading makes the surface Ce reduction becomes less favoured, requiring a higher temperature.

Despite this, gold must play a role in the redox behaviour and reducibility of the surface of AuCeCu sample. Even the presence of gold species with different oxidation states (Au^0, Au^{1+} and Au^{3+}) should not be discarded. In fact, there is no complete agreement in the literature about which is the main gold species (metallic or cationic) that generally improves the reducibility of Au/ceria based catalysts [63-67]. If produced, gold reduction would occur at low temperatures, probably overlapped with copper and surface Ce^{4+} events. The experimental H_2 consumption of the LTP is higher than the theoretical one necessary to reduce all gold (even considered as Au^{3+}) and copper species, (see Table 3), thus confirming the simultaneous gold, copper and surface cerium cations reduction processes at such temperature.

The redox behaviour at low temperature of the AuCeCu solid is complex, implying several reduction events at the same time. Indeed, the analysis of bimetallic Au-Cu systems has demonstrated the high solubility between both metals at different Au/Cu molar ratios [68], which supports the possibility of the formation of AuCu alloys, favoured under the reducing

atmosphere and the increasing of temperature during the TPR analysis, as recently demonstrated by in situ XRD in H_2 atmosphere studies [19].

The Au/Cu molar ratio becomes a key factor affecting the reducibility properties of the systems, as demonstrated Llorca et al. [22] in their work on propene epoxidation by N_2O over TiO_2-supported Au-Cu alloys catalysts. The solid with the lowest metal content (1.2 wt. %) and the lowest Au/Cu molar ratio (1/3) presented the maximum catalytic activity and the highest selectivity to epoxidation. This agrees with the results previously reported by Chimentão et al. [18] for similar catalysts with higher metallic content in the same reaction. They proposed that the copper content seemed to have a strong influence on dispersion and the catalytic performances of the metallic particles because, the higher the amount of copper, the lower the particle size of the metallic particles. However, when the calcination temperature increases, the surface of the AuCu alloy nanoparticles was progressively decorated with oxidized Cu species, which were detrimental for the redox behaviour and hence for the catalytic activity.

According to the last two cited reports, the addition of gold improved the redox behaviour at low temperature. However, Fonseca et al. [24] recently published a study about the cooperative effect of Au and Cu on ceria-modified catalysts for the PROX reaction where the opposite behaviour was exhibited. They observed that the reducibility of CeO_2 in the Au/CeO_2 and CuO_x/CeO_2 was superior to that of the $Au\text{-}CuO_x/CeO_2$. This was explained in terms of the modification of the initial reduction state of gold and copper species in the bimetallic system compared with the monometallic ones. This points out the possible modification of the electronic environment of the metallic nanoparticles when the Au-Cu interactions are established, decreasing in this case the reducibility of the system. The TPR profiles show in Figure 3 for the CeCu and AuCeCu solids agree with this explanation.

3.2. Catalytic performance and kinetic model

The performance of the catalysts for the oxidation of CO has been investigated evaluating the influence of the O_2 availability and the oxidizing-reducing conditions of the feed-stream. Thus, while the TOX reaction was performed in a large excess of O_2 (O_2/CO=6.2), a high concentration of H_2 was present under typical PROX conditions using a stoichiometric O_2/CO ratio (0.5). The CO conversion results for both reactions are depicted as a function of temperature in Figure 4.

Both solids achieve complete CO TOX conversion, although the gold catalyst allows reaching it at lower temperature (89 °C) thus evidencing that the CO oxidation ability of doped-ceria systems is enhanced by the deposition of small loadings of gold [14,24,69,70]. Since the AuCeCu sample presents a lower reducibility than the CeCu one (Figure 3), its higher activity cannot be related with this factor. Generally, the easier reduction of the material, associated with a higher amount of available reducible species and the lowering of their reduction temperature, plays an important role in the CO oxidation reaction since determines the ability of the material to exchange oxygen with the gas phase, which is crucial for the activation of the reactants over the catalyst surface during the process. In this case, however, the enhancement of the CO oxidation abilities should be related with the presence of Au itself. The surface sites associated to gold are very active and allow a more efficient activation of the reactants. These results are in good agreement with previous reports where ceria-based catalysts loaded with 1 wt. % gold exhibited good performances in the TOX reaction [40,70].

Concerning the PROX reaction, both catalysts show similar behaviours; the CO conversion increases with temperature up to very similar maxima at about 98 %. Nevertheless, the AuCeCu solid reached the highest CO conversion at lower temperature than the CeCu one (120 °C and 140 °C, respectively. The different catalytic performances under TOX and PROX reactions conditions highlight the relevance of the availability of reactants during the process. Although the CO oxidation is the common reaction for both processes, the feed-stream compositions are very different each other. That of PROX not only presented a lower concentration of O_2 but also contained H_2, which competes with CO for the active sites. This could be why the catalysts did not achieve 100% CO conversion under PROX conditions. Additionally both H_2 oxidation and R-WGS may be responsible for the observed decrease in CO conversion at temperatures higher than 120-140°C. These reactions are promoted by temperature and reduce the selectivity for CO oxidation of the global process [36,71]. According to these observations, although the AuCeCu catalyst allowed to achieve the maximum CO conversion at lower temperature, gold species and/or their interaction with the support could be improving also the side reactions, and this is why the activity of AuCeCu is lower than that of CeCu at relatively high temperatures (above 140 °C).

Taking into account the sensitivity of the catalysts to the composition of the reaction mixture, and in order to establish additional criteria for comparison between both catalysts, different feed-stream compositions have been tested in the PROX reaction over the AuCeCu solid (Table

1). These experiments consisted in the variation of the CO, O_2, H_2O and CO_2 concentrations, and allowed to establish a kinetic model for the gold catalyst based on the principles previously considered for the development of the kinetic model for the CeCu solid [36]. The experimental data of CO conversion and selectivity of the AuCeCu catalyst were fitted to the considered kinetic model according to the methodology presented in the experimental section [36,56]. Regarding the kinetic expressions for the H_2 oxidation (Eq. 8) and the R-WGS reactions (Eq. 9) with the gold catalyst, it was observed that the rate equations developed for the CeCu solid [36] remained valid. For obtaining a good description of the experimental data the rate expression for the CO oxidation over AuCeCu must include some adsorption terms (Eq. 10) in a similar way than for the CeCu catalyst [36]. However, although the catalytic behaviour of these two materials is similar, the adequate adsorption terms are not the same. In the case of the CeCu solid, adsorption terms due to CO, CO_2 and O_2 are included (Eq. 11), while that of CO is absent in the kinetic expression for the gold catalyst (Eq. 10). In the different rate expressions k_{CO}, k_{H_2} and $k_{R\text{-}WGS}$ are kinetic constants, P_i (i = CO, O_2, H_2, CO_2, H_2O) partial pressures, K_j (j = O_2, CO_2, CO) adsorption equilibrium constants and K_{WGS} is the equilibrium constant of the water-gas shift reaction. The estimated parameters are compiled in Table 4. Values of the kinetic and adsorption equilibrium constants are given at 100 °C. E_A stands for apparent activation energy and (-ΔH) for heat of adsorption.

$$-R_{H_2[AuCeCu]} = k_{H_2} \cdot P_{H_2} \cdot P_{O_2}^{0.5} \quad \text{(Eq. 8)}$$

$$-R_{R-WGS[AuCeCu]} = k_{R-WGS} \cdot (P_{H_2} \cdot P_{CO_2} - K_{WGS} \cdot P_{CO} \cdot P_{H_2O}) \quad \text{(Eq. 9)}$$

$$-R_{CO[AuCeCu]} = \frac{k_{CO} \cdot P_{CO} \cdot P_{O_2}^{0.5}}{(1 + K_{CO_2} \cdot P_{CO_2} + K_{O_2} \cdot P_{O_2}^{0.5})^2} \quad \text{(Eq. 10)}$$

$$-R_{CO[CeCu]} = \frac{k_{CO} \cdot P_{CO} \cdot P_{O_2}^{0.5}}{(1 + K_{CO} \cdot P_{CO} + K_{CO_2} \cdot P_{CO_2} + K_{O_2} \cdot P_{O_2}^{0.5})^2} \quad \text{(Eq. 11)}$$

The activation energy of the CO oxidation is reduced by about 7 kJ/mol in the presence of gold compared with the CeCu catalyst. This may be one of the reasons for the slightly high catalytic activity of the gold catalyst at low temperatures. Concerning the H_2 oxidation there is no variation of the kinetic parameters. Another positive effect of the incorporation of gold is on some adsorption parameters. On the one hand, the inhibiting effect of the CO adsorption disappears. On the other hand, the enthalpy of O_2 adsorption decreases which contributes to a significant decrease of the adsorption constant for oxygen. The interaction between gold and

the support, probably as bimetallic gold-copper species, allows a more efficient CO adsorption over the catalytic surface resulting in minimizing the contribution of such process to the reaction rate. On the other hand, the modification of the oxygen adsorption may be enhancing their availability not only for the CO oxidation but also for the H_2 consumption and this is why the AuCeCu is less active than the CeCu solid at higher temperatures when the second reaction is enhanced. The relevance of the adsorptions terms has been reported in other works on the PROX reaction. For instance Besser et al. [72] presented a kinetic model that was employed for comparing through modelling and simulation the effects of heat transfer limitations in microreactors and packed bed reactors for PROX.

López et al. [73] have highlighted the difficulties in finding a common basis of comparison regarding the performance of copper-based catalysts for the PROX reaction. These authors performed a comparative study including unsupported, ceria-supported and modified copper catalysts on the basis of a kinetic equation for CO oxidation over copper-ceria catalysts developed by Liu and Flytzani-Stephanopoulus [34]. In contrast with this expression, rate equations 10 and 11 include adsorption terms for CO_2 and oxygen whereas the power of their denominators is 2 instead of 1. We can perform a rough comparison of the kinetic constants at 100^{o}C taking into account typical initial values of the CO and O_2 partial pressures in our work, 0.01 atm and 0.005 atm, respectively, resulting in k_{CO} = 0.003 mol/(s·g_{cat}). In view of the very low dependence on the reactants pressure of the kinetic constants reported by López et al. [73], it can be concluded on the basis of the value of k_{CO} that the catalysts investigated in this study are among the most active copper-cerium catalysts for PROX reaction reported in the literature.

The comparison of the experimental data and the model fittings is presented in Figures 5 and 6. In these Figures, the CO conversion (Figures 5a and 6a) is showed along with the selectivity to the CO oxidation (Figures 5b and 6b) after varying the O_2 and CO concentrations in the feed-stream. In general, the model describes reasonably well the experimental data. This success in the kinetic model formulation is principally due to the consideration of the three reactions (CO and H_2 oxidation and R-WGS), as in the case of the CeCu solid [36].

Concerning the experimental results, whatever the O_2 concentration used, the CO conversion increases with temperature until reaching a maximum in the 100–200 °C region (Figure 5a). At high O_2 concentrations, complete CO conversion is achieved, which is not the case when the O_2 concentration (0.5 O_2 vol. %) is below the stoichiometric one. The selectivity to CO oxidation

(Figure 5b) decreases with temperature and with the O_2 concentration in the feed-stream. The effect of the temperature over the selectivity agrees with the observation of a region of maximum CO conversion (Figure 5a). At low temperatures the CO oxidation takes place very selectively, although the rate and the CO conversions, achieved are low. As the temperature increases, the H_2 oxidation starts to compete with that of CO. In addition, the R-WGS reaction is also favoured by the temperature increase, consuming H_2 and producing CO, and contributing that way to the observed negative effect on the overall process. As the O_2 concentration in the feed-stream increases the CO oxidation is enhanced, but also that of hydrogen. This fact may be both thermodynamic and kinetically detrimental for the R-WGS reaction due to the increased concentration of H_2O.

These trends of the CO conversion and selectivity results can be interpreted in terms of the estimated kinetic parameters. Indeed, the estimated activation energy for the H_2 oxidation is higher than that for the CO oxidation (110.1 and 30 kJ/mol respectively, Table 4). For that reason the CO oxidation is principally enhanced at lower temperatures, where the higher energetic barrier for the H_2 oxidation inhibits this side reaction. The kinetic model of the AuCeCu does not present important changes with respect to that of the CeCu solid, suggesting that the presence of gold does not alter significantly the mechanism of reaction. On the other hand, the catalytic results obtained after changing the CO concentration in the feed-stream and keeping constant the O_2 concentration (Figure 6) are similar to those obtained with the modification of the O_2 content (Figure 5), especially taking into account that, in this case, the O_2 concentrations are always above the stoichiometric value. When using a lower CO content, the conversion slightly increases, especially at temperatures below 150 °C. Additionally the selectivity to CO oxidation also decreases with temperature and the decrease of the CO content. As was described above, with a lower concentration of CO in the feed-stream, the O_2 availability in the reactor increases and consequently, the H_2 oxidation is enhanced.

The effect of the presence of CO_2 and H_2O in the feed-stream is shown in Figure 7. This is important for the development of any catalysts for the PROX reaction because this is a cleaning process of the H_2 produced by reforming of organic molecules that also produces CO_2 and H_2O. Therefore their presence is hardly avoidable under real operating conditions. Additionally they may be competing for adsorption over the active sites required for the oxidation reactions and may induce deactivation processes. At temperatures below 150 °C, the CO conversion decreases as the CO_2 concentration in the feed-stream increases (Figure 7a); this effect is less pronounced at higher temperatures. Such behaviour demonstrates that the

addition of CO_2 produces a negative effect on the catalytic activity. This is reflected in the kinetic model by a large value of the heat of CO_2 adsorption (79.8 kJ/mol). A similar behaviour was previously described for the CeCu system [47]. From these results, and since no changes in selectivity were observed, it could be inferred that CO_2 is adsorbed competitively with CO, as reported early for CuO_x/CeO_2 catalysts [26,47], decreasing that way the CO conversion. Also, we can conclude that the presence of gold does not modify the CO_2 adsorption properties of the catalyst. On the other hand, although the kinetic model captures the general tendency of the experimental data, a significant discrepancy with the measured values in the presence of CO_2 is noticeable. This disagreement increases with the increase of the CO_2 concentration in the feed-stream and can be related with the stable adsorption of carbonaceous species over the catalysts surface, which is favoured at high CO_2 contents. The formation of these species over the catalyst surface was not considered during the formulation of the kinetic model and probably, a term to describe it would be needed in order to fully match these experimental data. However, no additional detriment of the CO conversion was observed after the inclusion of H_2O along with CO_2 (see Figure 7b). This tolerance to the presence of H_2O was previously described for the CeCu system [36] and is in agreement with that described by other authors for Cu-Ce, Co-Ce and Cu-Zr fluorite oxide composite catalysts [35].

4. Conclusions

The results obtained in this study allow drawing some conclusions regarding the behaviour of gold catalysts for the CO PROX reaction.

The interaction of gold with the CeCu mixed oxide strongly depends on the oxygen vacancies population of this material. The interaction of this noble metal with the oxygen vacancies seems to produce electronic transfers that are enhancing the reduction of the surface at temperatures lower than for the CeCu solid.

The results of the kinetic study carried out over the AuCeCu catalyst suggest that the presence of gold mainly influences the CO adsorption process during the PROX reaction. This fact may be associated to the surface electronic activity produced by the interaction of the cationic species that would create more active sites for the CO adsorption.

Finally, the deposition of a small amount of gold (1 wt. %) results beneficial for the CO oxidation in TOX and PROX, but in the second reaction such effect is counteracted by the low O_2 availability and the presence of H_2, CO_2 and H_2O that favour side reactions and compete with CO for being adsorbed over the active sites of the catalysts.

5. Acknowledgements

Financial support for this work has been obtained from the Spanish Ministry of Science and Innovation and Ministry of Economy and Competitiveness (ENE2009-14522-C05 and ENE2012-37431-C03-03, respectively) co-financed by FEDER funds from the European Union, and from Junta de Andalucía (P09-TEP-5454). O.H. Laguna thanks the same Ministry for the FPI fellowship (BES-2007-14409) awarded.

6. References

[1] Demirbas A. Potential applications of renewable energy sources, biomass combustion problems in boiler power systems and combustion related environmental issues. Prog Energ Combust 2005;31:171-192

[2] Sopena C, Diéguez PM, Sáinz D, Urroz JC, Guelbenzu E, Gandía LM. Conversion of a commercial spark ignition engine to run on hydrogen: Performance comparison using hydrogen and gasoline. Int J. Hydrogen Energ 2010;35:1420-1429

[3] Arzamendi G, Diéguez PM, Montes M, Centeno MA, Odriozola JA, Gandía LM. Integration of methanol steam reforming and combustion in a microchannel reactor for H_2 production: A CFD simulation study. Catal Today 2009;143:25-31

[4] Burch R, Gold catalysts for pure hydrogen production in the water-gas shift reaction: Activity, structure and reaction mechanism. Phys Chem Chem Phys 2006;8:5483-5500

[5] Idakiev V, Tabakova T, Tenchev K, Yuan Z-Y, Ren T-Z, Su B-L. Gold nanoparticles supported on ceria-modified mesoporous titania as highly active catalysts for low-temperature water-gas shift reaction. Catal Today 2007;128:223-229

[6] Tabakova T, Idakiev V, Papavasiliou J, Avgouropoulos G, Ioannides T. Effect of additives on the WGS activity of combustion synthesized CuO/CeO_2 catalysts. Catal Commun 2007;8:101-106

[7] Yuan Z-Y, Idakiev V, Vantomme A, Tabakova T, Ren T-Z, Su B-L. Mesoporous and nanostructured CeO_2 as supports of nano-sized gold catalysts for low-temperature water-gas shift reaction. Catal Today 2008;131:203-210

[8] Mariño F, Baronetti G, Laborde M, Bion N, Le Valant A, Epron F, Duprez D. Optimized $CuO-CeO_2$ catalysts for CO-PROX reaction. Int J Hydrogen Energ 2008;33:1345-1353

[9] Holladay JD, Hu J, King DL, Wang Y. An overview of hydrogen production technologies. Catal Today 2009;139:244-260

[10] Korotkikh O, Farrauto R. Selective catalytic oxidation of CO in H_2: fuel cell applications. Catal Today 2000;62:249-254

[11] Abu-Zied BM, Soliman SA. Thermal decomposition of praseodymium acetate as a precursor of praseodymium oxide catalyst. Thermochim Acta. 2008;470:91-97

[12] Chen L, Ma D, Zhang Z, Guo Y, Ye D, Huang B. Low Pt Loading High Catalytic Performance of PtFeNi/Carbon Nanotubes Catalysts for CO Preferential Oxidation in Excess Hydrogen I: Promotion Effects of Fe and/or Ni. Catal Lett 2012;142:1-9

[13] Wörner A, Friedrich C, Tamme R. Development of a novel Ru-based catalyst system for the selective oxidation of CO in hydrogen rich gas mixtures. App Catal A-Gen 2003;245: 1-14

[14] Laguna OH, Romero-Sarria F, Centeno MA, Odriozola JA. Gold supported on metal-doped ceria catalysts (M = Zr, Zn and Fe) for the preferential oxidation of CO (PROX). J Catal 2010;276:360-370

[15] Tabakova T, Avgouropoulos G, Papavasiliou J, Manzoli M, Boccuzzi F, Tenchev K, Vindigni F, Ioannides T. CO-free hydrogen production over Au/CeO_2-Fe_2O_3 catalysts: Part 1. Impact of the support composition on the performance for the preferential CO oxidation reaction. App Catal B-Environ 2011;101:256-265

[16] Avgouropoulos G, Ioannides T, Matralis HK, Batista J, Hocevar S. CuO-CeO_2 mixed oxide catalysts for the selective oxidation of carbon monoxide in excess hydrogen. Catal Lett 2001;73:33-40

[17] Gamarra D, Hornés A, Koppány Z, Schay Z, Munuera G, Soria J, Martínez-Arias A, Catalytic processes during preferential oxidation of CO in H_2-rich streams over catalysts based on copper-ceria. J Power Sources 2007;169:110-116

[18] Chimentão RJ, Medina F, Fierro JLG, Llorca J, Sueiras JE, Cesteros Y, Salagre P. Propene epoxidation by nitrous oxide over Au–Cu/TiO_2 alloy catalysts. J Mol Cat A-Chem 2007;274:159-168

[19] Liu X, Wang A, Li L, Zhang T, Mou C-Y, Lee J-F. Structural changes of Au–Cu bimetallic catalysts in CO oxidation: In situ XRD, EPR, XANES, and FT-IR characterizations. J Catal 2011;278:288-296

[20] Liu X Wang A, Wang X, Mou C-Y, Zhang T. Au-Cu Alloy nanoparticles confined in SBA-15 as a highly efficient catalyst for CO oxidation. Chem Commun 2008;27:3187-3189

[21] Liu X, Wang A, Zhang T, Su D-S, Mou C-Y. Au–Cu alloy nanoparticles supported on silica gel as catalyst for CO oxidation: Effects of Au/Cu ratios. Catal Today 2011;160:103-108

[22] Llorca J, Domínguez M, Ledesma C, Chimentão RJ, Medina F, Sueiras J, Angurell I, Seco M, Rossell O. Propene epoxidation over TiO_2-supported Au–Cu alloy catalysts prepared from thiol-capped nanoparticles. J Catal 2008;258:187-198

[23] Mozer TS, Dziuba DA, Vieira CTP, Passos FB. The effect of copper on the selective carbon monoxide oxidation over alumina supported gold catalysts. J Power Sources 2009;187: 209-215

[24] Fonseca J, Ferreira HS, Bion N, Pirault-Roy L, Rangel MdC, Duprez D, Epron F. Cooperative effect between copper and gold on ceria for CO-PROX reaction. Catal Today 2012;180:34-41

[25] Aguilar-Guerrero V, Gates BC. Kinetics of CO oxidation catalyzed by highly dispersed CeO_2-supported gold. J Catal 2008;260:351-357

[26] Caputo T, Lisi L, Pirone R, Russo G. Kinetics of the preferential oxidation of CO over CuO/CeO_2 catalysts in H_2-rich gases. Ind Eng Chem Res 2007;46:6793-6800.

[27] Choi Y, Stenger HG. Kinetics, simulation and insights for CO selective oxidation in fuel cell applications. J Power Sources 2004;129: 246-254

[28] Davran-Candan T, Demir M, Yildirim R. Analysis of reaction mechanisms and kinetics of preferential CO oxidation over $Au/\gamma\text{-}Al_2O_3$. React Kinet Mech Cat 2011;104:1-10

[29] Lee HC, Kim DH. Kinetics of CO and H_2 oxidation over $CuO\text{-}CeO_2$ catalyst in H_2 mixtures with CO_2 and H_2O. Catal Today 2008;132:109-116

[30] Schumacher B, Denkwitz Y, Plzak V, Kinne M, Behm RJ. Kinetics, mechanism, and the influence of H_2 on the CO oxidation reaction on a Au/TiO_2 catalyst. J Catal 2004;224:449-462.

[31] Sedmak G, Hočevar S, Levec J. Kinetics of selective CO oxidation in excess of H_2 over the nanostructured $Cu_{0.1}Ce_{0.9}O_{2-\gamma}$ catalyst. J Catal 2003;213:135-150

[32] Sedmak G, Hočevar S, Levec J. Transient kinetic model of CO oxidation over a nanostructured $Cu_{0.1}Ce_{0.9}O_{2-\gamma}$ catalyst. J Catal 2004;222:87-99

[33] Chen G, Yuan Q, Li H, Li S. CO selective oxidation in a microchannel reactor for PEM fuel cell. Chem Eng J 2004;101:101-106

[34] Liu W, Flytzani-Stephanopoulos M. Total Oxidation of Carbon-Monoxide and Methane over Transition Metal Fluorite Oxide Composite Catalysts: II. Catalyst Characterization and Reaction-Kinetics. J Catal 1995;153:317-332

[35] Liu W, Flytzani-Stephanopoulos M. Total Oxidation of Carbon Monoxide and Methane over Transition Metal Fluorite Oxide Composite Catalysts: I. Catalyst Composition and Activity. J Catal 1995;153:304-316

[36] Arzamendi G, Uriz I, Diéguez PM, Laguna OH, Hernández WY, Álvarez A, Centeno MA, Odriozola JA, Montes M, Gandía LM. Selective CO removal over Au/CeFe and CeCu catalysts in microreactors studied through kinetic analysis and CFD simulations. Chem Eng J 2011;167:588-596

[37] Cruz S, Sanz O, Poyato R, Laguna OH, Echave FJ, Almeida LC, Centeno MA, Arzamendi G, Gandía LM, Souza-Aguiar EF, Montes M, Odriozola JA. Design and testing of a microchannel reactor for the PROX reaction. Chem Eng J 2011;167:634-642

[38] Centeno MA, Portales C, Carrizosa I, Odriozola JA. Gold supported CeO_2/$Al2O_3$ catalysts for CO oxidation: influence of the ceria phase. Catal Lett 2005;102:289-297

[39] Penkova A, Chakarova K, Laguna OH, Hadjiivanov K, Saria FR, Centeno MA, Odriozola JA. Redox chemistry of gold in a Au/FeO_x/CeO_2 CO oxidation catalyst. Catal Commun 2009;10:1196-1202

[40] Laguna OH, Centeno MA, Romero-Sarria F, Odriozola JA. Oxidation of CO over gold supported on Zn-modified ceria catalysts. Catal Today 2011;172:118-123

[41] Rase H.F. Fixed-bed reactor design and diagnostics: gas-phase reactions. 1st ed. Michigan University: Butterworth MA. 1990, p. 106

[42] Nelder JA, Mead R. A Simplex Method for Function Minimization. Comput J 1965;7:308-313

[43] Nelder JA, Mead RA. Errata. Comput J 1965;8:27-27

[44] Lite DR. CRC Handbook of Chemistry and Physics. 84th ed. New York: CRC Pres. LCL 2003

[45] Kónya Z, Puntes VF, Kiricsi I, Zhu J, Ager JW, Ko MK, Frei H, Alivisatos P, Somorjai GA. Synthetic Insertion of Gold Nanoparticles into Mesoporous Silica. Chem Mater 2003;15:1242-1248

[46] Zhu P, Li J, Zuo S, Zhou R. Preferential oxidation properties of CO in excess hydrogen over CuO-CeO_2 catalyst prepared by hydrothermal method. App Surf Sci 2008;255:2903-2909

[47] Jobbágy M, Mariño F, Schönbrod B, Baronetti G, Laborde M. Synthesis of copper-promoted CeO_2 catalysts. Chem Mater 2006;18:1945-1950

[48] Mariño F, Schönbrod B, Moreno M, Jobbágy M, Baronetti G, Laborde M. CO preferential oxidation over CuO-CeO_2 catalysts synthesized by the urea thermal decomposition method. Catal Today 2008;133-135:735-742

[49] Hernández WY, Centeno MA, Romero-Sarria F, Odriozola JA. Synthesis and characterization of $Ce_{1-x}Eu_xO_{2-x/2}$ mixed oxides and their catalytic activities for CO oxidation. J Phys Chem C 2009;113:5629-5635

[50] Spanier JE, Robinson RD, Zhang F, Chan SW, Herman IP. Size-dependent properties of CeO_{2-y} nanoparticles as studied by Raman scattering. Phys Rev B 2001;64:2454071-2454078

[51] Fornasiero P, Balducci G, Di Monte R, Kašpar J, Sergo V, Gubitosa G, Ferrero A, Graziani M. Modification of the Redox Behaviour of CeO_2 Induced by Structural Doping with ZrO_2. J Catal 1996;164:173-183

[52] Laguna OH, Centeno MA, Boutonnet M, Odriozola JA. Fe-doped ceria solids synthesized by the microemulsion method for CO oxidation reactions. App Catal B-Environ 2011;106:621-629

[53] Hernández WY, Romero-Sarria F, Centeno MA, Odriozola JA. In situ characterization of the dynamic gold-support interaction over ceria modified Eu^{3+}. Influence of the oxygen vacancies on the co oxidation reaction. J Phy Chem C 2010;114:10857-10865

[54] Graham GW, Weber WH, Peters CR, Usmen R. Empirical method for determining CeO_2-particle size in catalysts by raman spectroscopy. J Catal 1991;130:310-313

[55] Xiao G, Li S, Li H, Chen L. Synthesis of doped ceria with mesoporous flowerlike morphology and its catalytic performance for CO oxidation. Microp and Mesop Mat 2009;120:426-431

[56] Ganduglia-Pirovano MV, Hofmann A, Sauer J. Oxygen vacancies in transition metal and rare earth oxides: Current state of understanding and remaining challenges. Surf Sci Rep 2007;62:219-270

[57] Liu Z, Zhou R, Zheng X. Preferential Oxidation of CO in Excess Hydrogen over CuO-CeO_2 Catalyst Prepared by Chelating Method. J Nat Gas Chem 2007;16:167-172

[58] Martínez-Arias A, Fernández-García M, Gálvez O, Coronado JM, Anderson JA, Conesa JC, Soria J, Munuera G. Comparative Study on Redox Properties and Catalytic Behavior for CO Oxidation of CuO/CeO_2 and CuO/$ZrCeO_4$ catalysts. J Catal 2000;195:207-216

[59] Martínez-Arias A, Gamarra D, Fernández-García M, Wang XQ, Hanson JC, Rodríguez JA. Comparative study on redox properties of nanosized CeO_2 and CuO/CeO_2 under CO/O_2. J Catal 2006;240:1-7

[60] Gellings PJ, Bouwmeester HJM. Ion and mixed conducting oxides as catalysts. Catal Today 1992;12:1-101

[61] Sirichaiprasert K, Luengnaruemitchai A, Pongstabodee S. Selective oxidation of CO to CO_2 over Cu-Ce-Fe-O composite-oxide catalyst in hydrogen feed stream. Int J Hydrogen Energ 2007;32:915-926

[62] Araújo VD, Bellido JDA, Bernardi MIB, Assaf JM, Assaf EM. CuO-CeO_2 catalysts synthesized in one-step: Characterization and PROX performance. Int J Hydrogen Energ 2012;37:5498-5507

[63] Amieiro Fonseca A, Fisher J, Ozkaya D, Shannon M, Thompsett D. Ceria-zirconia supported Au as highly active low temperature Water-gas shift catalysts. Top Catal 2007;44:223-235

[64] Fu Q, Saltsburg H, Flytzani-Stephanopoulos M. Active nonmetallic Au and Pt species on ceria-based water-gas shift catalysts. Science 2003;301:935-938

[65] Jacobs G, Ricote S, Patterson PM, Graham UM, Dozier A, Khalid S, Rhodus E, Davis BH. Low temperature water-gas shift: Examining the efficiency of Au as a promoter for ceria-based catalysts prepared by CVD of a Au precursor. App Catal A-Gen 2005;292:229-243

[66] Karpenko A, Leppelt R, Plzak V, Behm RJ. The role of cationic Au^{3+} and nonionic Au^0 species in the low-temperature water-gas shift reaction on Au/CeO^2 catalysts. J Catal 2007;252:231-242

[67] Kim CH, Thompson LT. Deactivation of Au/CeOx water gas shift catalysts. J Catal 2005;230:66-74

[68] De G, Rao CNR. Two-dimensional Au and Au-Cu alloy nanocrystals with orientation in (111) plane embedded in glassy silica films. J Phys Chem B 2003;107:13597-13600

[69] Fonseca J, Royer S, Bion N, Pirault-Roy L, Rangel MdC, Duprez D, Epron F. Preferential CO oxidation over nanosized gold catalysts supported on ceria and amorphous ceria-alumina. App Catal B-Environ 2012;128:10-20

[70] Laguna OH, Centeno MA, Arzamendi G, Gandía LM, Romero-Sarria F, Odriozola JA. Iron-modified ceria and Au/ceria catalysts for Total and Preferential Oxidation of CO (TOX and PROX). Catal Today 2010;157:155-159

[71] Roberts GW, Chin P, Sun X, Spivey JJ. Preferential oxidation of carbon monoxide with Pt/Fe monolithic catalysts: interactions between external transport and the reverse water-gas-shift reaction. App Catal B-Environ 2003;46:601-611

[72] Ouyang X, Besser RS. Effect of reactor heat transfer limitations on CO preferential oxidation. J Power Sources 2005;141:39-46

[73] López I, Valdés-Solís T, Marbán G. An attempt to rank copper-based catalysts used in CO-PROX reaction. Int J Hydrogen Energ 2008;33:2008:197–205

TABLES

Table 1. Feed-stream compositions (vol. %) used for the kinetic experiments with the AuCeCu catalyst during the PROX reaction

Compositions	CO	O_2	H_2	CO_2	H_2O	N_2
Com. 1	2.0	0.5	50.0	--	--	47.5
Com. 2	2.0	1.5	50.0	--	--	46.5
Com. 3	2.0	3.0	50.0	--	--	45.0
Com. 4	0.3	1.0	50.0	--	--	48.7
Com. 5	0.5	1.0	50.0	--	--	48.5
Com. 6	1.0	1.0	50.0	--	--	48.0
Com. 7	1.0	1.0	50.0	2.0	--	46.0
Com. 8	1.0	1.0	50.0	5.0	--	43.0
Com. 9	1.0	1.0	50.0	10.0	--	38.0
Com. 10	1.0	1.0	50.0	2.0	10.0	36.0

Table 2. Chemical composition and textural properties of the studied materials

Solids	CuO (wt. %)	Cu (at. %)	Au (wt. %)	BET surface area (m^2/g)	Pore volume (cm^3/g)	Average pore size (Å)
CeCu	15.0	27.6	--	76	0.136	73.4
AuCeCu	12.3	23.4	0.9	68	0.193	102

Table 3. Theoretical and experimental H_2 consumption of the LTP in the TPR analysis of the prepared catalysts

Solids	Experimental H_2 consumption [LTP] (μmol H_2/g_{cat})	Theoretical H_2 consumption [LTP] (μmol H_2/g_{cat})		
		Assuming (Cu^{2+})	Assuming (Cu^{2+} + Au^{+})	Assuming (Cu^{2+} + Au^{3+})
CeCu	2372.6	1960.8	--	--
AuCeCu	1617.6	1557.6	1580.7	1610.7

Table 4. Estimated kinetic parameters of the rate equations for the PROX process over the CeCu and AuCeCu catalysts[(a)]

Parameter	CeCu [36]	AuCeCu
k_{CO} [mol/(s·g_{cat}·$atm^{1.5}$)]	4.15	4.15
$E_{A,CO}$ [kJ/mol]	36.9	30.0
K_{CO} [atm^{-1}]	8.7	--
$(-\Delta H)_{CO}$ [kJ/mol]	11.0	--
K_{CO_2} [atm^{-1}]	1.12×10^{3}	1.12×10^{3}
$(-\Delta H)_{CO_2}$ [kJ/mol]	79.8	79.8
K_{O_2} [$atm^{-0.5}$]	219.0	145.1
$(-\Delta H)_{O_2}$ [kJ/mol]	1.7	0.3
k_{H_2} [mol/(s g_{cat}·$atm^{1.5}$)]	8.9×10^{-7}	2.1×10^{-6}
E_{A,H_2} [kJ/mol]	110.0	110.1
$k_{R\text{-}WGS}$ [mol/(s·g_{cat}·atm^{2})]	5×10^{-9}	5×10^{-9}
$E_{A,R\text{-}WGS}$ [kJ/mol]	36.9	36.9

[(a)] Values of the kinetic and adsorption equilibrium constants are given at 100 °C

FIGURE CAPTIONS

Figure 1. XRD patterns of the studied catalysts

Figure 2. Raman spectra of the studied catalysts

Figure 3. TPR profiles of the prepared catalysts

Figure 4. CO conversion during the TOX and the PROX reactions over the CeCu and AuCeCu catalysts

Figure 5. Effect of the O_2 concentration in the feed-stream during the PROX reaction over the AuCeCu catalyst: a) CO conversion; b) Selectivity to CO oxidation. (Symbols are the experimental data and dashed lines the kinetic model fit)

Figure 6. Effect of the CO concentration in the feed-stream during the PROX reaction over the AuCeCu catalyst: a) CO conversion; b) Selectivity to CO oxidation. (Symbols are the experimental data and dashed lines the kinetic model fit)

Figure 7. Effects of CO_2 and H_2O on the CO conversion over the AuCeCu catalyst: a) Modifying of the CO_2 concentration; b) Addition of H_2O (Symbols are the experimental data and dashed lines the kinetic model fit)

FIGURES

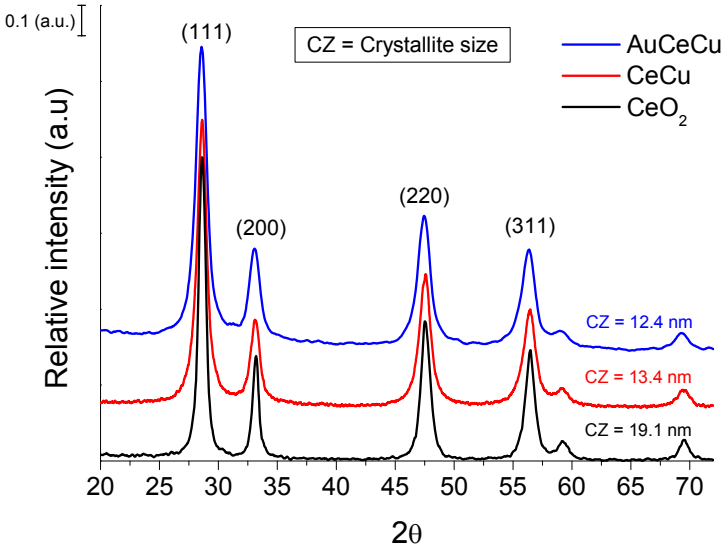

Figure 1

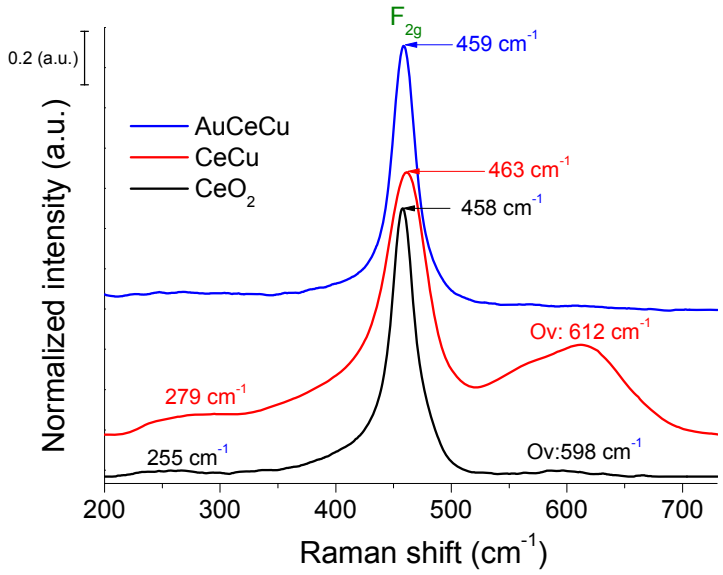
F2g
459 cm-1
0.2 (a.u.)
AuCeCu
CeCu
CeO2
463 cm-1
458 cm-1
Ov: 612 cm-1
279 cm-1
255 cm-1
Ov:598 cm-1
Normalized intensity (a.u.)
200
300
400
500
600
700
Raman shift (cm-1)

Figure 2

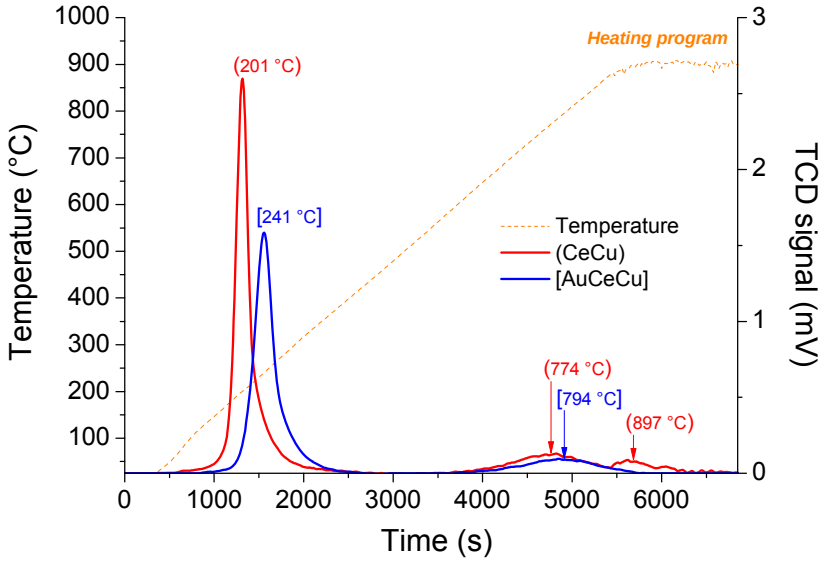
Heating program
(201 °C)
[241 °C]
Temperature
(CeCu)
[AuCeCu]
(774 °C)
[794 °C]
(897 °C)
Temperature (°C)
TCD signal (mV)
Time (s)
1000
900
800
700
600
500
400
300
200
100
0
1000
2000
3000
4000
5000
6000
3
2
1
0

Figure 3

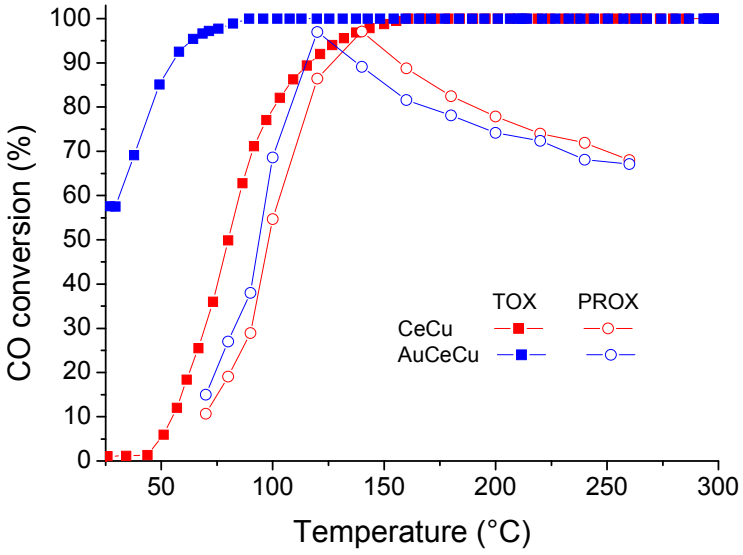
CO conversion (%)
Temperature (°C)
TOX
PROX
CeCu
AuCeCu
0
10
20
30
40
50
60
70
80
90
100
50
100
150
200
250
300

Figure 4

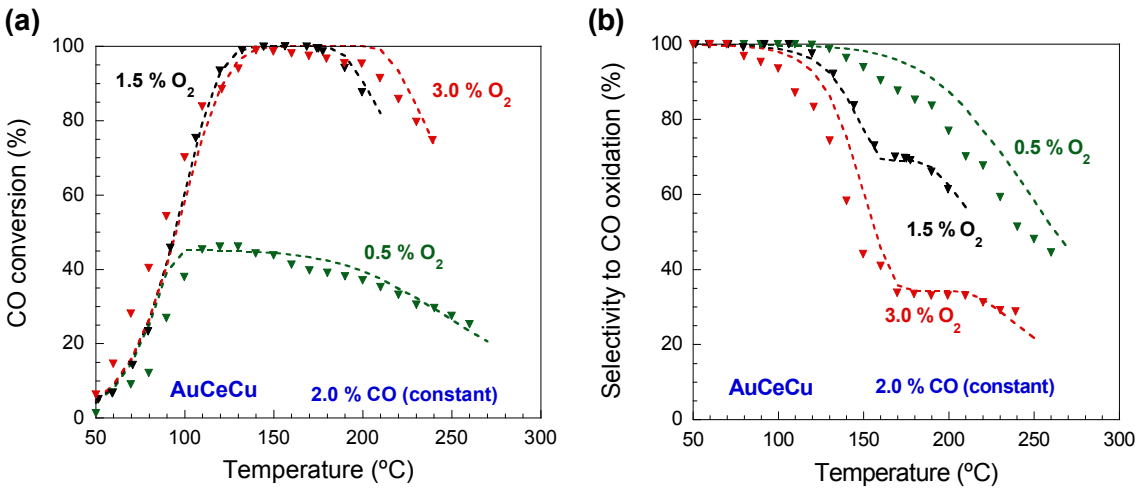
(a)
CO conversion (%)
Temperature (ºC)
1.5 % O2
3.0 % O2
0.5 % O2
AuCeCu
2.0 % CO (constant)
(b)
Selectivity to CO oxidation (%)
Temperature (ºC)
0.5 % O2
1.5 % O2
3.0 % O2
AuCeCu
2.0 % CO (constant)

Figure 5

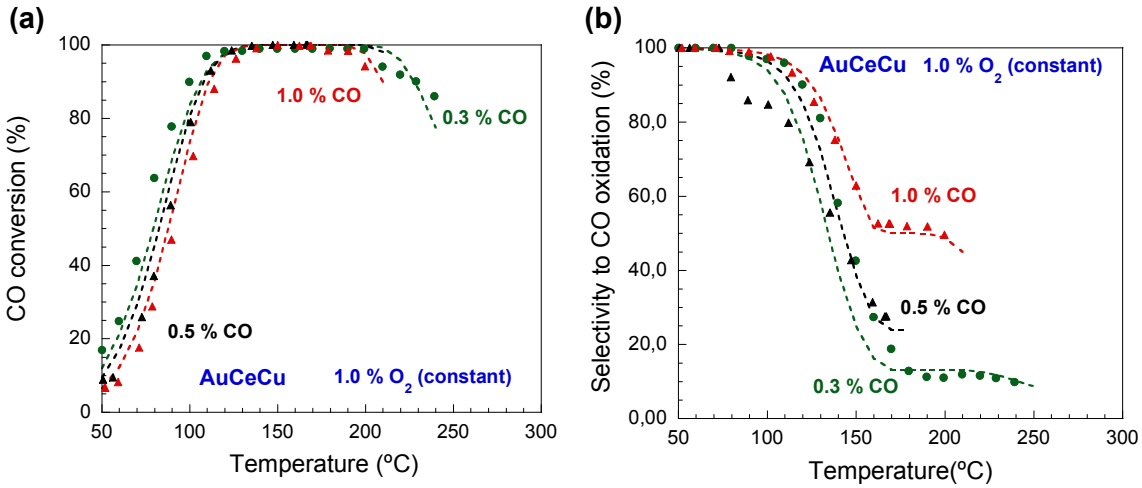
(a)
CO conversion (%)
Temperature (°C)
1.0 % CO
0.3 % CO
0.5 % CO
AuCeCu
1.0 % O2 (constant)
(b)
Selectivity to CO oxidation (%)
Temperature(°C)
AuCeCu
1.0 % O2 (constant)
1.0 % CO
0.5 % CO
0.3 % CO

Figure 6

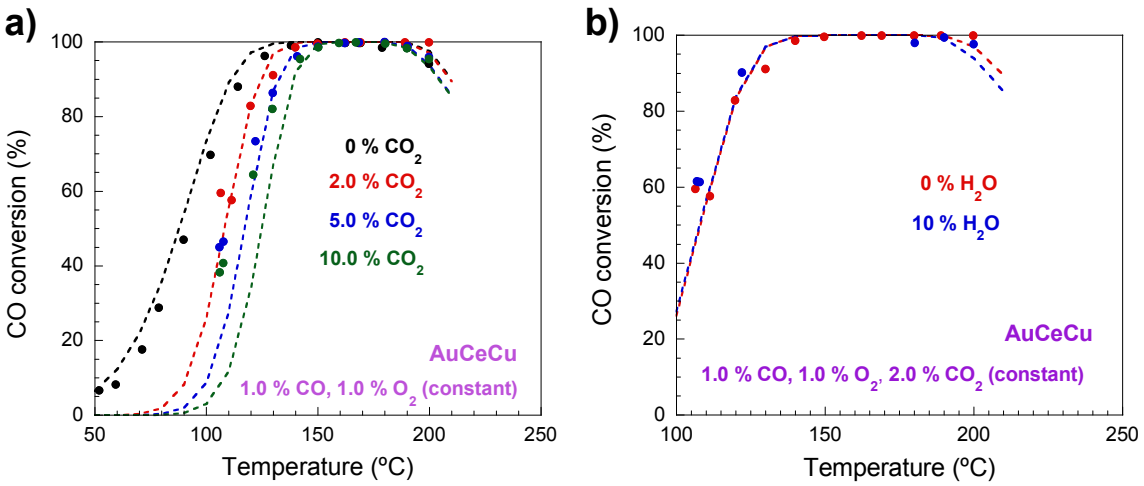
a)
CO conversion (%)
Temperature (ºC)
0 % CO2
2.0 % CO2
5.0 % CO2
10.0 % CO2
AuCeCu
1.0 % CO, 1.0 % O2 (constant)
b)
CO conversion (%)
Temperature (ºC)
0 % H2O
10 % H2O
AuCeCu
1.0 % CO, 1.0 % O2, 2.0 % CO2 (constant)

Figure 7